

# TMEM150C/Tentonin3 Is a Regulator of Mechano-gated Ion Channels

Evan O. Anderson,<sup>1</sup> Eve R. Schneider,<sup>1</sup> Jon D. Matson,<sup>1</sup> Elena O. Gracheva,<sup>1,2,3</sup> and Sviatoslav N. Bagriantsev<sup>1,4,\*</sup>

<sup>1</sup>Department of Cellular & Molecular Physiology, Yale University School of Medicine, New Haven, CT 06520, USA

<sup>2</sup>Department of Neuroscience, Yale University School of Medicine, New Haven, CT 06520, USA

<sup>3</sup>Program in Cellular Neuroscience, Neurodegeneration and Repair, Yale University School of Medicine, New Haven, CT 06520, USA

<sup>4</sup>Lead Contact

\*Correspondence: [slav.bagriantsev@yale.edu](mailto:slav.bagriantsev@yale.edu)

<https://doi.org/10.1016/j.celrep.2018.03.094>

## SUMMARY

Neuronal mechano-sensitivity relies on mechano-gated ion channels, but pathways regulating their activity remain poorly understood. TMEM150C was proposed to mediate mechano-activated current in proprioceptive neurons. Here, we studied functional interaction of TMEM150C with mechano-gated ion channels from different classes (Piezo2, Piezo1, and the potassium channel TREK-1) using two independent methods of mechanical stimulation. We found that TMEM150C significantly prolongs the duration of the mechano-current produced by all three channels, decreases apparent activation threshold in Piezo2, and induces persistent current in Piezo1. We also show that TMEM150C is co-expressed with Piezo2 in trigeminal neurons, expanding its role beyond proprioceptors. Finally, we cloned TMEM150C from the trigeminal neurons of the tactile-foraging domestic duck and showed that it functions similarly to the mouse ortholog, demonstrating evolutionary conservation among vertebrates. Our studies reveal TMEM150C as a general regulator of mechano-gated ion channels from different classes.

## INTRODUCTION

Somatosensory ganglia of vertebrates contain various types of mechano-sensitive neurons, including low- and high-threshold mechano-receptors and proprioceptors. These neurons can convert mechanical stimulation into ionic current due to the presence of mechano-gated ion channels, including nonselective excitatory channels, such as by Piezo2, and potassium-selective inhibitory channels, such as TREK-1 ( $K_{2p2.1}$ ) (Alloui et al., 2006; Ranade et al., 2015). Activity of these channels is regulated through alternative splicing, interaction with the cytoskeleton, signaling pathways, and the lipid composition of the plasma membrane (Anderson et al., 2017; Borbiri and Rohacs, 2017; Murthy et al., 2017; Szczot et al., 2017). Despite recent advances, proteins and pathways involved in regulation of mechano-sensitivity remain poorly understood. Identification of

novel mechano-gated ion channels and their modulators is essential for understanding mechano-sensitivity in somatic cells and neurons.

Piezo2 generates fast-inactivating mechano-evoked current (MA current) in neurons from trigeminal (TG) and dorsal root ganglia (DRG). The deletion of Piezo2 abrogates fast MA current in light touch mechano-receptors and proprioceptors without affecting mechano-sensitivity in neurons with intermediately and slowly inactivating MA currents (Ranade et al., 2014; Woo et al., 2015). TMEM150C/Tentonin3 was proposed to act as an ion channel mediating slowly inactivating MA current in proprioceptive neurons in mouse DRG (Hong et al., 2016). Recently, it was shown that heterologous expression of TMEM150C fails to generate MA current in cells with genomic ablation of the *PIEZO1* gene (Dubin et al., 2017). Here, we tested the hypothesis that TMEM150C acts as a modulator of mechano-sensitivity, rather than an ion channel, by studying its effects on MA current in cells expressing bona fide mechano-gated channels from different classes: Piezo1, Piezo2, and the potassium-selective channel TREK-1.

## RESULTS

### TMEM150C Stimulates Piezo2 Mechano-current

TMEM150C has been reported to function in proprioceptors from mouse DRG (Hong et al., 2016), which also express Piezo2 (Florez-Paz et al., 2016; Woo et al., 2015). To test whether TMEM150C is co-expressed with Piezo2 in other types of somatosensory neurons, we analyzed distribution of TMEM150C in adult duck TG, a ganglion devoid of proprioceptors but rich in Piezo2-expressing mechano-receptors (84.5% of all neurons) (Schneider et al., 2017; Schneider et al., 2014). Using RNA *in situ* hybridization, we found that  $83.3\% \pm 1.0\%$  (19 TG sections, 2,808 total cells) of duck TG neurons express TMEM150C (Figures 1A and 1B). The abundance of TMEM150C and Piezo2-positive neurons in duck TG necessitates an overlap between the two neuronal populations, suggesting that TMEM150C is co-expressed with Piezo2 outside of proprioceptors.

We and others have hypothesized that TMEM150C could act as a modulator of Piezo channel function (Dubin et al., 2017). To test this, we measured whole-cell MA current in cells co-expressing mouse TMEM150C (mTMEM150C) and mouse Piezo2 in response to mechanical stimulation with a glass probe (Hao and Delmas, 2011). To avoid potential confounding effects of



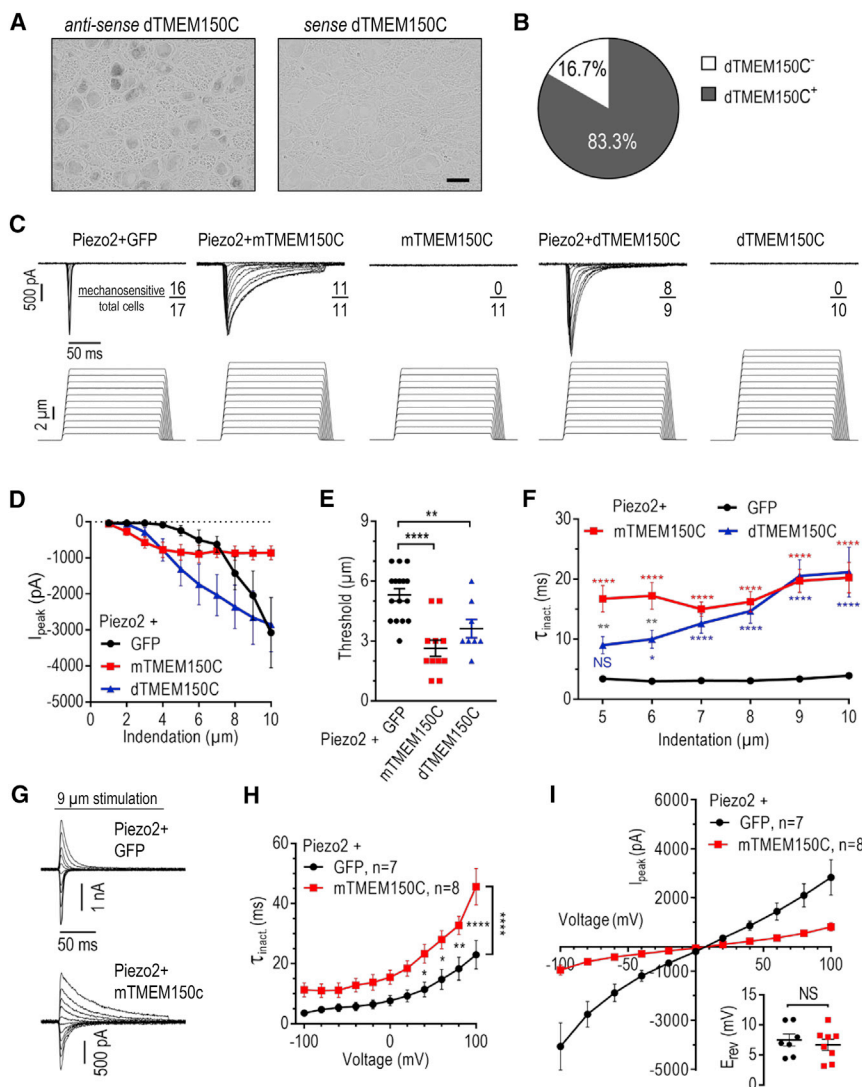


**Figure 1. Mouse and Duck TMEM150C Potentiate Piezo2 Mechano-current in HEK293T<sup>ΔP1</sup> Cells**

(A and B) Representative images of RNA *in situ* hybridization (A) and quantification of TMEM150C-expressing neurons (B) in adult duck TG (2,808 cells from 19 TG sections from 2 animals). Scale bar, 50  $\mu$ m.

(C) Exemplar whole-cell MA current traces recorded in HEK293T<sup>ΔP1</sup> cells expressing Piezo2 with or without mouse or duck TMEM150C in response to mechanical indentation with a glass probe to the indicated depth ( $E_{\text{hold}} = -80$  mV).

(D) Peak MA current measured at different indentation depths in HEK293T<sup>ΔP1</sup> cells expressing indicated constructs ( $E_{\text{hold}} = -80$  mV). Data shown as mean  $\pm$  SEM.

(E) Quantification of MA current activation threshold ( $p < 0.0001$ , one-way ANOVA with Dunnett's correction, \*\* $p < 0.001$ , \*\*\*\* $p < 0.0001$ ). Data shown as mean  $\pm$  SEM.

(F) Quantification of MA current inactivation rate ( $\tau_{\text{inact}}$ ) measured at different indentation depths (ordinary two-way ANOVA with Bonferroni correction,  $p < 0.0001$  for expression construct effect; NS, not significant;  $p > 0.05$ , \* $p < 0.05$ , \*\* $p < 0.01$ , \*\*\*\* $p < 0.0001$ ; red, blue, and gray asterisks indicate statistical comparisons between, respectively, Piezo2/mTMEM150C and Piezo2/mTMEM150C and Piezo2/dTMEM150C and Piezo2/dTMEM150C). Data shown as mean  $\pm$  SEM.

(G) Representative traces of whole-cell MA currents evoked in response to 9  $\mu$ m mechanical indentation at different voltages from  $-100$  mV to 100 mV, in 20 mV increments.

(H) Quantification of MA current  $\tau_{\text{inact}}$  at different voltages (two-way ANOVA with Sidak's correction, \* $p < 0.05$ , \*\* $p < 0.01$ , \*\*\*\* $p < 0.0001$ ). Data shown as mean  $\pm$  SEM.

(I) Peak MA current-voltage plots in response to mechanical indentation of 5–10  $\mu$ m for Piezo2/GFP and 4–9  $\mu$ m for Piezo2/mTMEM150C. The inset shows quantification of the reversal potential  $E_{\text{rev}}$  (unpaired t test; NS, not significant;  $p > 0.05$ ). Data shown as mean  $\pm$  SEM.

See also Figures S1, S3A, and S3B.

endogenous MA current, we used HEK293T cells carrying a genomic ablation of the *PIEZO1* gene (HEK293T<sup>ΔP1</sup>) (Dubin et al., 2017; Lukacs et al., 2015). Co-expression of Piezo2 with GFP yielded typical fast-inactivating MA current, while the expression of mouse TMEM150C alone produced no mechanical response (Figures 1C, 1D, and S1A). However, co-expression of Piezo2 with TMEM150C produced a twofold decrease in the onset of detectable MA current (apparent activation threshold) from  $5.3 \pm 0.3$   $\mu$ m to  $2.6 \pm 0.4$   $\mu$ m ( $p = 0.0001$ , Dunnett's test) (Figure 1E). Additionally, TMEM150C co-expression led to a fivefold prolongation in the rate of MA current inactivation ( $\tau_{\text{inact}}$ ) at all indentation depths that consistently produced MA current in both groups (5–10  $\mu$ m), from 3.4–3.9 ms to 16.7–20.3 ms, respectively (two-way ANOVA,  $p < 0.0001$  for expression construct effect) (Figure 1F). The effect did not depend on the amount of channel molecules on the surface, as we observed

an increase in  $\tau_{\text{inact}}$  independently of peak MA current amplitude (Figure S1B).

We also tested a TMEM150C ortholog cloned from TG of tactile specialist duck. Duck TMEM150C (dTMEM150C) is 87% identical to the mouse protein (Figure S1C). When expressed alone, duck TMEM150C did not confer mechano-sensitivity to HEK293T<sup>ΔP1</sup> cells (Figures 1C, 1D, and S1A). Upon co-expression with Piezo2, duck TMEM150C significantly decreased the apparent threshold of mechanical activation from  $5.3 \pm 0.3$   $\mu$ m to  $3.6 \pm 0.5$   $\mu$ m ( $p = 0.0098$ , Dunnett's test) and prolonged  $\tau_{\text{inact}}$  in the 5–10  $\mu$ m indentation range from 3.4–3.9 ms to 9.0–21.2 ms (two-way ANOVA,  $p < 0.0001$  for expression construct and voltage effects) (Figures 1E and 1F).

To understand whether the resultant MA current retained properties characteristic of Piezo2 alone, we analyzed voltage dependence of  $\tau_{\text{inact}}$ . The inactivation rate of Piezo2 MA current

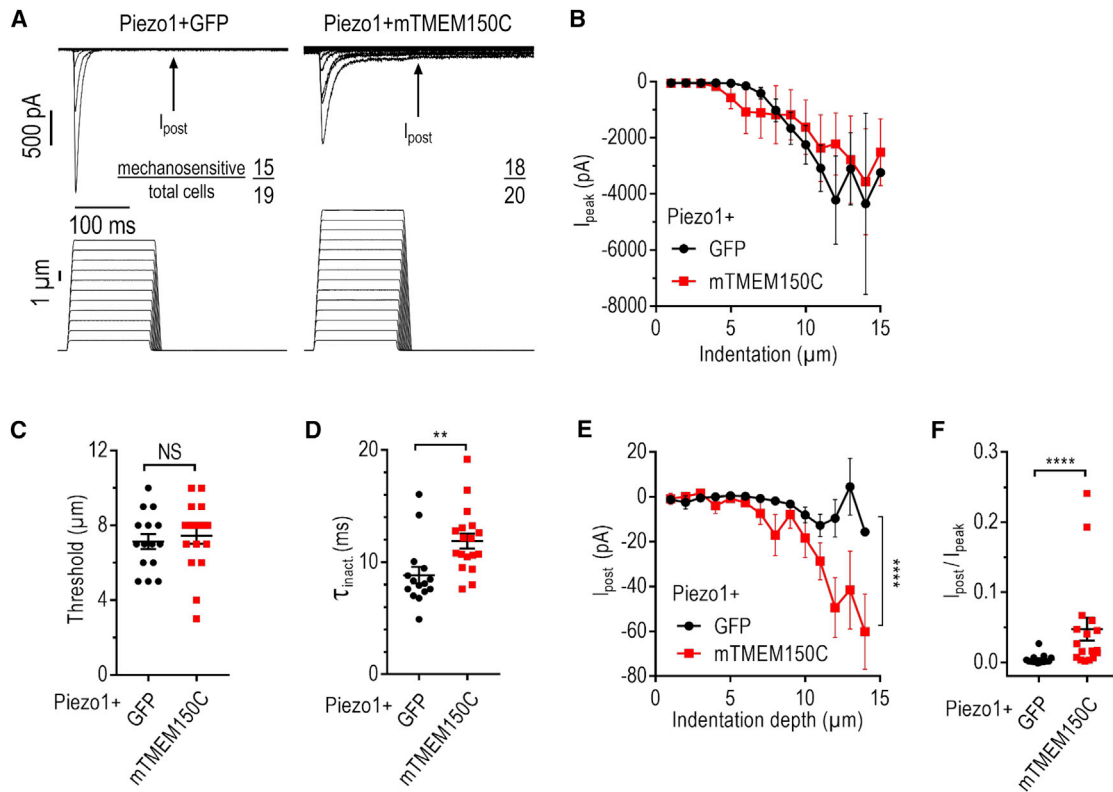


**Figure 2. TMEM150C Potentiates MA Current Produced by Piezo1**

(A) Exemplar whole-cell MA current traces recorded in HEK293T<sup>ΔP1</sup> cells in response to mechanical indentation with a glass probe at  $E_{hold} = -80$  mV. Arrow indicates the position of persistent post-stimulus MA current measurement.  
 (B) Peak MA current measured at different indentation depths in HEK293T<sup>ΔP1</sup> cells expressing indicated constructs ( $E_{hold} = -80$  mV). Data shown as mean  $\pm$  SEM.  
 (C and D) Quantification of MA current activation threshold (C) and inactivation rate  $\tau_{inact}$  (D). NS, not significant;  $p > 0.05$ , \*\* $p < 0.01$ ; unpaired *t* test (C) and Mann-Whitney *U*-test (D). Data shown as mean  $\pm$  SEM.  
 (E) Post-stimulus MA current amplitude at different indentation depths. \*\*\*\* $p < 0.0001$  for expression construct effect, two-way ANOVA. Data shown as mean  $\pm$  SEM.  
 (F) Quantification of peak-normalized amplitude of persistent post-stimulus MA current. \*\*\*\* $p < 0.0001$ , Mann-Whitney *U* test. Data shown as mean  $\pm$  SEM. See also Figure S2A.

increases with depolarization 6.4-fold, from  $3.6 \pm 0.6$  ms at  $-100$  mV to  $23.0 \pm 4.7$  ms at  $100$  mV (two-way ANOVA,  $p < 0.0001$  for voltage effect) (Coste et al., 2010; Wu et al., 2017b). We found a similarly significant fourfold increase in  $\tau_{inact}$  in cells co-expressing Piezo2 and mouse TMEM150C, from  $11.3 \pm 2.3$  ms at  $-100$  mV to  $45.7 \pm 6.1$  ms at  $100$  mV (two-way ANOVA,  $p < 0.0001$  for voltage effect) (Figures 1G and 1H). Additionally, co-expression with TMEM150C did not change the reversal potential of the resultant MA current (Figures 1I and S1D).

Together, our observations show that MA current produced by co-expression of TMEM150C and Piezo2 has similar voltage dependence of inactivation and ion selectivity but significantly augmented activation threshold and inactivation kinetics compared to MA current produced by Piezo2 alone. Although these data do not exclude the possibility that TMEM150C is an ion channel active in the presence of another mechano-transducer (Hong et al., 2017), they suggest more strongly that TMEM150C is a positive modulator of Piezo2-mediated me-

chano-current. The similarity between the effects of duck and mouse TMEM150C suggest that the function of this protein is conserved among vertebrates.

### TMEM150C Potentiates Piezo1 Mechano-current Independently of Stimulation Method

To test whether the observed effects are specific to Piezo2, we co-expressed TMEM150C with Piezo1, a homolog of Piezo2 that mediates mechano-responses in somatic cells (Murthy et al., 2017) and neural stem cells (Pathak et al., 2014) and guides axon growth in the developing brain (Koser et al., 2016). When expressed alone in HEK293T<sup>ΔP1</sup> cells, mouse Piezo1 produces fast-inactivating MA current (Figures 2A, 2B, and S2A). Co-expression with mouse TMEM150C did not change the apparent activation threshold ( $7.1 \pm 0.4$   $\mu$ m and  $7.4 \pm 0.4$   $\mu$ m for Piezo1 alone and with TMEM150C, respectively,  $p = 0.61$ , *t* test) (Figure 2C) but significantly prolonged the average  $\tau_{inact}$ , from  $8.1 \pm 0.7$  ms to  $11.9 \pm 0.7$  ms ( $p = 0.0012$ , Mann-Whitney *U* test) (Figure 2D). Importantly, in the presence of TMEM150C,

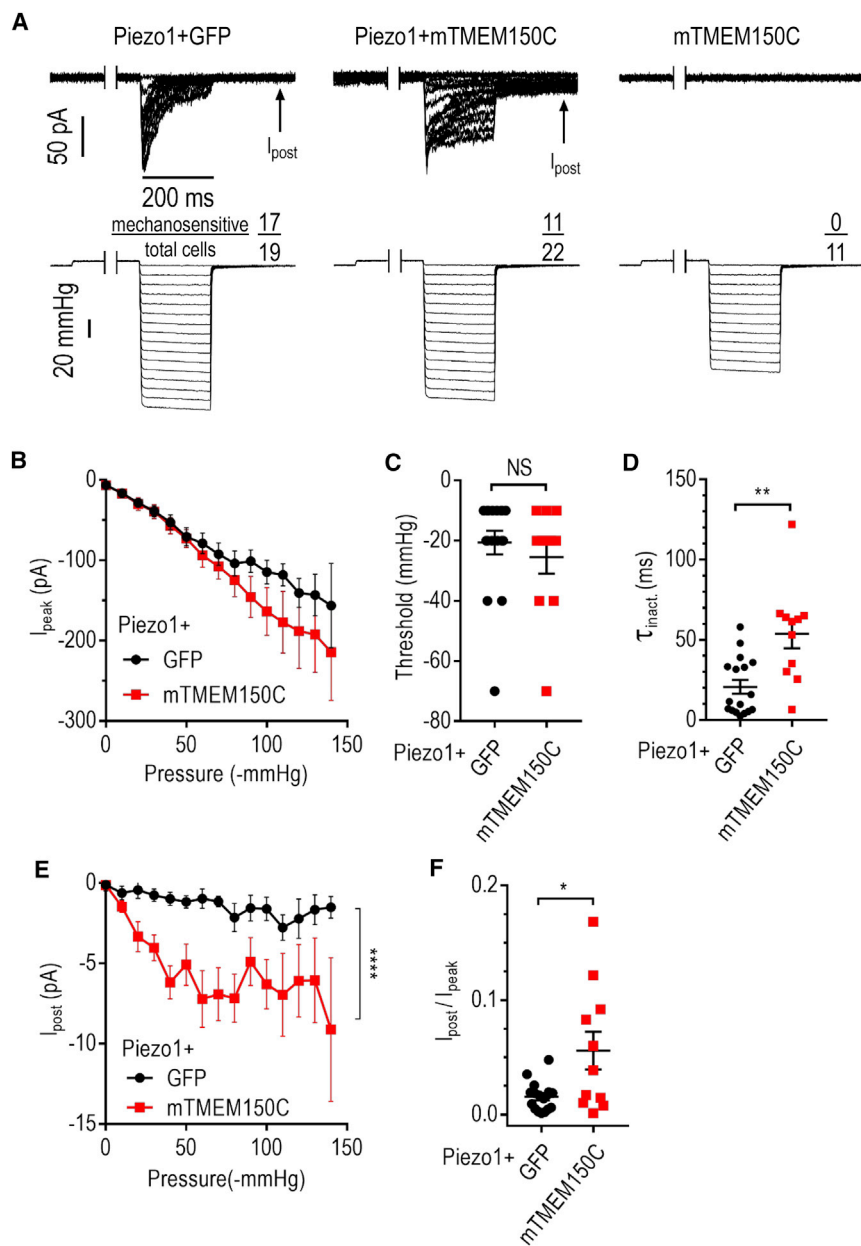


### Figure 3. TMEM150C Potentiates Piezo1 MA Current Evoked by High-Speed Pressure Clamp

(A) Exemplar cell-attached MA current traces recorded in HEK293T<sup>AP1</sup> cells in response to application of a negative pressure in the pipette at  $E_{\text{hold}} = -60$  mV. Each pressure step was preceded by a 500-ms step at 5 mmHg to remove inactivation. Arrow indicates the position of persistent post-stimulus MA current measurement.

(B) Quantification of peak MA current amplitude measured at  $-60$  mV at different pressures. Data shown as mean  $\pm$  SEM.

(C and D) Quantification of MA current activation threshold (C) and inactivation rate  $\tau_{\text{inact}}$  (D). NS, not significant;  $p > 0.05$ , \*\* $p < 0.01$ ; Mann-Whitney *U*-test (C) and unpaired *t* test (D). Data shown as mean  $\pm$  SEM.

(E) Post-stimulus MA current amplitude at different pressures. \*\*\*\* $p < 0.0001$  for expression construct effect, two-way ANOVA. Data shown as mean  $\pm$  SEM.

(F) Quantification of peak-normalized amplitude of persistent post-stimulus MA current. \* $p < 0.05$ , Welch's test. Data shown as mean  $\pm$  SEM. See also Figure S2B.

MA current persisted beyond the removal of mechanical stimulation ( $I_{\text{post}}$ ; Figures 2E and 2F). This is consistent with an earlier observation documenting the presence of the persistent post-stimulus current upon expression of TMEM150C in wild-type HEK293T cells, which also express a small amount of endogenous Piezo1 (Dubin et al., 2017; Hong et al., 2016).

We wondered if the prolongation of inactivation and the induction of persistent post-stimulus current depend on the method of mechanical stimulation. Unlike Piezo2, Piezo1 can be activated by the application of mechanical force in a cell-attached patch using high-speed pressure clamp (HSPC) (Besch et al., 2002; Gottlieb et al., 2012). While we did not detect mechano-evoked activity in cells expressing TMEM150C alone, Piezo1-expressing

cells produced robust MA current (Figures 3A and 3B). Co-expression of the two proteins did not change the apparent activation threshold ( $-20.6 \pm 3.9$  mmHg and  $-25.5 \pm 5.5$  mmHg for Piezo1 alone and with mTMEM150C, respectively,  $p = 0.37$ , Mann-Whitney *U*-test) (Figure 3C), but produced more than 2.6 fold increase in average  $\tau_{\text{inact}}$  from  $20.7 \pm 4.3$  ms to  $53.9 \pm 9.1$  ms ( $p = 0.0011$ , *t* test) (Figures 3D and S2B). The HSPC approach produced a larger increase in  $\tau_{\text{inact}}$  than stimulation with a glass probe, possibly due to perturbations in the lipid composition, basal tension, and mechanics of the plasma membrane caused by the formation of the gigaseal (Gottlieb et al., 2012; Suchyna et al., 2009). Additionally, co-expression with TMEM150C generated persistent post-stimulus current (Figures 3E and 3F). Overall, our findings with HSPC-mediated stimulation are consistent with those obtained through indentation of HEK293T<sup>AP1</sup> cells with a glass probe, demonstrating that the observed effects are independent of the method of mechanical stimulation.

Together, our data show that co-expression with TMEM150C prolongs inactivation kinetics of Piezo2 and Piezo1. However, we only detected a decrease in threshold with Piezo2 and the induction of persistent post-stimulus current with Piezo1. The absence of the persistent post-stimulus current at negative potentials in any condition other than upon co-expression of Piezo1 with TMEM150C (also see below) suggests that it is specific to this combination of proteins. The presence of channel-specific

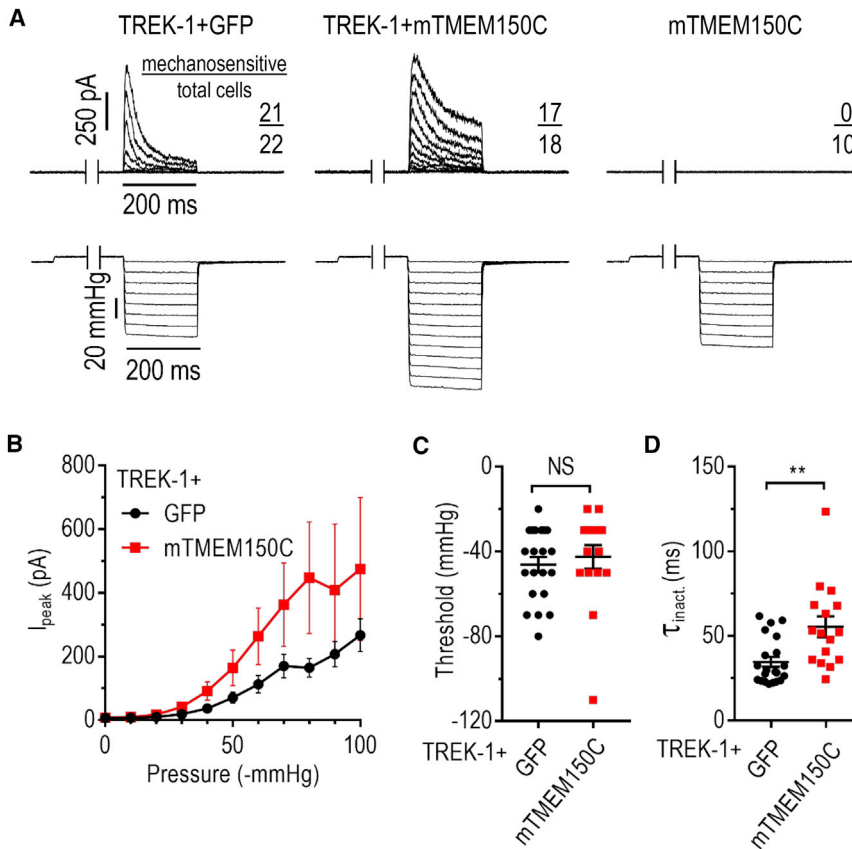


**Figure 4. TMEM150C Potentiates MA Current of Potassium-Selective TREK-1 Channel**

(A) Exemplar cell-attached MA current traces recorded in HEK293T<sup>ΔP1</sup> cells in response to application of a negative pressure in the pipette using a high-speed pressure clamp ( $E_{\text{hold}} = 0$  mV). Each pressure step was preceded by a 500-ms step at 5 mmHg to remove inactivation.

(B) Quantification of peak MA potassium current amplitude measured at  $E_{\text{hold}} = 0$  mV at different pressures. Data shown as mean  $\pm$  SEM.

(C and D) Quantification of cell-attached MA current activation threshold (C) and average inactivation rate (D). NS, not significant;  $p > 0.05$ , \*\* $p < 0.01$ , Mann-Whitney  $U$  test. Data shown as mean  $\pm$  SEM.

See also [Figures S2C](#) and [S3C](#).

effects further supports the idea that TMEM150C is a modulator of Piezo channels.

### TMEM150C Enhances Mechano-current Produced by TREK-1

To determine whether TMEM150C expression modulates other types of mechano-transducers, we tested the mechano-gated potassium-selective channel TREK-1. Like Piezo2, TREK-1 is abundantly expressed in somatosensory neurons and is physiologically important for mechano-sensitivity (Alloui et al., 2006; Nořl et al., 2009). Mechanical stimulation of HEK293T<sup>ΔP1</sup> cells expressing mouse TREK-1 by HSPC at 0 mV produced outward potassium-selective MA current with slow inactivation, whereas cells expressing mouse TMEM150C alone did not exhibit mechano-activity (Figures 4A and 4B). Co-expression of TREK-1 with TMEM150C did not change apparent activation threshold ( $-46.2 \pm 3.7$  mmHg and  $-40.6 \pm 5.1$  mmHg for TREK-1 alone TREK-1 with TMEM150C, respectively,  $p = 0.15$ , Mann-Whitney  $U$  test) (Figure 4C) but significantly prolonged the average  $\tau_{\text{inact}}$  from  $34.7 \pm 3.0$  ms to  $55.4 \pm 6.1$  ms ( $p = 0.0013$ , Mann-Whitney  $U$  test) (Figures 4D and S2C). Importantly, we measured MA current at a holding potential of 0 mV, which permits the efflux of potassium via TREK-1 but restricts the net current from a nonselective cation channel, a role originally proposed for TMEM150C (Hong et al., 2016, 2017). Thus, similar to Piezo2 and Piezo1, TREK-1 MA current is enhanced by co-expression with TMEM150C.

In agreement with the functional data, we found that TMEM150C co-immunoprecipitates with TREK-1 and Piezo2, suggesting that TMEM150C can form a complex with the ion channels or exist in the same lipid domain (Figure S3). To test TMEM150C function more broadly, we used mouse  $K_v1.1$ , a voltage-gated potassium channel with a role in neuronal mechano-sensitivity (Hao et al., 2013). However, co-expression with TMEM150C did not affect voltage dependence of activation of  $K_v1.1$ , and the channel did not co-immunoprecipitate with TMEM150C (Figure S4). Together, our data show that TMEM150C is a modulator of different classes of mechano-gated ion channels.

### DISCUSSION

Here, we sought to understand the role of TMEM150C in the generation of mechano-activated current. We show, in agreement with previous observations, that TMEM150C expression does not produce MA current when expressed alone in HEK293T<sup>ΔP1</sup> cells (Dubin et al., 2017). Additionally, we demonstrate that TMEM150C expression prolongs the kinetics of MA current inactivation when co-expressed with Piezo1, Piezo2, or TREK-1, independently of the method of mechanical stimulation. When TMEM150C and TREK-1 are co-expressed, the resultant current is mediated by potassium, as expected if it was solely produced by TREK-1. Thus, our data strongly suggest that TMEM150C is a regulator of mechano-gated ion channels rather than a nonselective ion channel itself, as initially suggested (Hong et al., 2016).

Inactivation rate is a key element of mechano-gated channel function that determines the amount of excitatory (or inhibitory) in the case of TREK-1) flux of ions and ultimately influences generation of the action potential. Prolongation of Piezo1 and Piezo2  $\tau_{\text{inact}}$  has been linked to several pathological conditions, including hereditary xerocytosis (Bae et al., 2013; Glogowska et al., 2017), dehydrated hereditary stomatocytosis (Albuissou

et al., 2013), and distal arthrogryposis (Coste et al., 2013; Murthy et al., 2017). What could be the mechanism of TMEM150C-mediated prolongation of  $\tau_{\text{inact}}$  in such different ion channel classes? The Piezos and TREK-1 share no similarity in terms of amino acid sequence or overall structure (Guo and MacKinnon, 2017; Lolico et al., 2014, 2017; Saotome et al., 2017; Zhao et al., 2018). Piezo1 is directly activated by stretch in membrane blebs (Cox et al., 2016) and in a lipid bilayer (Syeda et al., 2016), and so is TREK-1 (Brohawn et al., 2014; Clausen et al., 2017). Interestingly, single-channel activity of reconstituted Piezo1 does not substantially decay after mechanical stimulation, suggesting that inactivation in cells may require additional components not present in the tested bilayer (Syeda et al., 2016). Aside from post-translational modifications, these components could include lipids and transmembrane or intracellular proteins, such as components of the cytoskeleton (Anderson et al., 2017; Borbiro and Rohacs, 2017; Murthy et al., 2017; Wu et al., 2017a). We propose that TMEM150C influences at least one such component, leading to changes in mechano-evoked responses in the Piezos and TREK-1.

We show that co-expression with TMEM150C significantly decreases the apparent activation threshold of Piezo2. The effect is not caused by increased channel expression, because at higher indentations, the magnitudes of Piezo2 current with and without mouse TMEM150C become similar. We hypothesize that the change in threshold stems, at least partially, from an increase in the channel's sensitivity to mechanical stimulation. This threshold change could in part be driven by the large prolongation of Piezo2 inactivation kinetics upon co-transfection with TMEM150C, giving rise to current that is detectable at lower stimulation. In this case, the absence of an effect of TMEM150C on Piezo1 and TREK-1 threshold could stem from a milder increase in  $\tau_{\text{inact}}$  compared to Piezo2, and larger initial  $\tau_{\text{inact}}$ . We therefore do not exclude the possibility that TMEM150C also produces a small decrease in activation threshold in these channels.

A TMEM150C homolog TMEM150A influences phospholipid homeostasis via interaction with phosphatidylinositol 4-kinase type III $\alpha$ , a key enzyme generating phosphatidylinositol 4-phosphate on the plasma membrane (Chung et al., 2015). Conceivably, TMEM150C could alter chemical composition of the plasma membrane, changing its mechanical properties, such as rigidity and tension. Tension alone, however, is unlikely to be the major factor regulating  $\tau_{\text{inact}}$ , as stepwise application of a negative pressure increases membrane tension proportionally, yet  $\tau_{\text{inact}}$  remains steady across a wide range of pressures (Lewis and Grandl, 2015; Wu et al., 2017b). Lipid content, on the other hand, can have a profound effect on ion channel function either directly, or via redistribution of the channels into membrane subdomains, and this was shown for the Piezos and TREK-1 (Bae et al., 2013; Borbiro et al., 2015; Comoglio et al., 2014; Qi et al., 2015; Sandoz et al., 2011). If a lipid-modulating role is confirmed for TMEM150C, then we should expect to see an effect of this protein on other ion channels and membrane proteins, even though we did not detect an effect on voltage dependence of  $K_v1.1$  activation.

Though important for physiology, the mechanism of activation and inactivation in Piezos and  $K_{2\text{ps}}$  is poorly understood. In Piezos, the magnitude of  $\tau_{\text{inact}}$  is dictated by the C-terminal extracel-

lular domain (CED), which forms a cap-like structure above the extracellular pore (Guo and MacKinnon, 2017; Saotome et al., 2017; Zhao et al., 2018). Reciprocal transposition of CED between Piezo1 and Piezo2 changes their  $\tau_{\text{inact}}$  accordingly (Wu et al., 2017b). The apparent absence of inactivation in reconstituted Piezo1 suggests that even though CED is a key element of the inactivation mechanism, it requires other components. Indeed, inactivation of the Piezos can be influenced pharmacologically, by mutations, and via destruction of the cytoskeleton (Coste et al., 2013; Cox et al., 2016; Syeda et al., 2015). Interestingly, TREK channels also possess an extracellular cap-like structure (Brohawn et al., 2012; Dong et al., 2015; Lolico et al., 2014, 2017), but its role in mechano-gating remains obscure. Studies identified the intracellular C terminus as a major modulator of gating via allosteric communication with the selectivity filter-based gate (Bagriantsev et al., 2011, 2012; Lolico et al., 2014; Schewe et al., 2016). Even though the architecture of the channels appear strikingly different, the similarity between the effects of TMEM150C on Piezo1, Piezo2, and TREK-1 suggests the existence of common principles governing mechano-gated channel opening and inactivation. Understanding how TMEM150C works could help reveal such mechanism.

TMEM150C was shown to have a role in proprioceptors, which also express Piezo2 (Hong et al., 2016). We now show that TMEM150C is expressed in 83.3% of neurons from TG of tactile specialist ducks, where proprioceptors are absent and the majority of cells are Piezo2-expressing touch receptors. The overlap between TMEM150C and Piezo2-expressing neurons may explain the prevalence of MA current with intermediate and slow inactivating kinetics in duck TG compared to mice or visually foraging chicken (Schneider et al., 2014, 2017). TMEM150C is also present in peptidergic and non-peptidergic nociceptors expressing Piezo2 (Borbiro et al., 2015; Prato et al., 2017). Since, as we show here, TMEM150C is a positive regulator of Piezo2 function, it is possible that in addition to proprioception, TMEM150C could also have a regulatory effect on light touch detection, heat, and mechano-nociception. However, behavioral tests using *Tmem150C* knockout mice only revealed deficits in motor coordination, consistent with TMEM150C expression in proprioceptors, while light touch and mechanical pain responses remained normal (Hong et al., 2016). Possibly, TMEM150C activity varies between different types of somatosensory neurons, such that the knockout may not have an equally significant impact on the function of light touch receptors and nociceptors as on proprioceptors. It is also possible that TMEM150C's effects are heterogeneous with regard to different splicing isoforms of Piezo2 (Szczoł et al., 2017), which could have preferential expression in specific types of somatosensory neurons. TREK-1 is broadly expressed in the somatosensory system, where it is thought to counterbalance excitation by generating mechanically induced potassium efflux (Alloui et al., 2006; Noël et al., 2009). Since TMEM150C prolongs TREK-1 MA current, the effect of *Tmem150C* knockout on light touch via suppression of Piezo2 could be mitigated by simultaneous suppression of the inhibitory activity of TREK-1 (Brohawn et al., 2014). Importantly, TMEM150C is also present in the CNS (Hong et al., 2016), suggesting that the observed effects of *Tmem150C* knockout on behavior could have a more complex explanation, involving

alterations in signal processing or brain development (Koser et al., 2016). Cell-type-specific knockouts are needed to reveal a role for TMEM150C in mechano-sensitivity.

## EXPERIMENTAL PROCEDURES

Further details and outlines of resources can be found in [Supplemental Experimental Procedures](#).

### Animals

Tissues from adult domestic ducks, which were raised and slaughtered for the purpose of human consumption and not for this study, were purchased post-mortem at MarWin Farm.

### RNA *In Situ* Hybridization

TGs were fixed in paraformaldehyde, sectioned at 12–15  $\mu\text{m}$ , probed with digoxigenin-labeled cRNA, and developed with alkaline-phosphatase-conjugated anti-digoxigenin Fab fragments.

### Immunoprecipitation

HEK293<sup>ΔP1</sup> cells were lysed in a buffer containing 1% CHAPS. Proteins were captured by antibodies immobilized on magnetic beads and analyzed by western blotting.

### Electrophysiology

Electrophysiology data were collected from HEK293T<sup>ΔP1</sup> cells. For whole-cell recordings of MA current, cells held at  $-80$  mV were stimulated with a glass probe in 1- $\mu\text{m}$ , 150-ms steps with a velocity of 1,000  $\mu\text{m}/\text{s}$  with 5 s between sweeps. For cell-attached recordings, membrane patches held at  $-60$  mV for Piezo1 or 0 mV for TREK-1 were subjected to stepwise, 200-ms negative pressure steps ( $\Delta 10$  mmHg) preceded by a 500-ms pre-pulse at 5 mmHg, with 3 s between stimuli. For Kv1.1 recordings, cells were stepped from  $-70$  mV to 30 mV ( $\Delta 10$  mV) from  $-70$  mV holding potential. For details on electrophysiology and solution compositions, see [Supplemental Experimental Procedures](#).

### Statistical Analysis

Data were obtained from at least two independent experiments and are reported as mean  $\pm$  SEM. Statistical tests were chosen based on normality of distributions and variance equality, or lack thereof, and the number of samples, are reported in figure legends.

## DATA AND SOFTWARE AVAILABILITY

The accession number for the domestic duck (mallard) TMEM150C is GenBank: MG697237.

## SUPPLEMENTAL INFORMATION

Supplemental Information includes Supplemental Experimental Procedures and four figures and can be found with this article online at <https://doi.org/10.1016/j.celrep.2018.03.094>.

## ACKNOWLEDGMENTS

We thank Pietro De Camilli and members of the Gracheva and Bagriantsev laboratories for their contributions throughout the project and Ardem Patapoutian for the gift of mPiezo2 plasmid and HEK293<sup>ΔP1</sup> cells. E.O.A. is an Edward L. Tatum fellow and was supported by the Gruber Foundation. E.R.S. is a postdoctoral fellow of the Arnold and Mabel Beckman Foundation. This study was partly funded by NIH grant 1R01NS091300-01A1 (to E.O.G.) and by NSF CAREER grant 1453167 and NIH NINDS grant 1R01NS097547-01A1 (to S.N.B.).

## AUTHOR CONTRIBUTIONS

E.O.A. designed and performed the majority of electrophysiological experiments and data analysis, with contributions from E.R.S. E.O.G. performed

RNA *in situ* hybridization. E.O.G. and J.D.M. performed cloning. S.N.B. performed immunoprecipitation. E.O.A., E.O.G., and S.N.B. wrote the manuscript. E.O.G. and S.N.B. conceived the study and provided supervision throughout the project.

## DECLARATION OF INTERESTS

The authors declare no competing financial interests.

Received: January 3, 2018

Revised: February 21, 2018

Accepted: March 20, 2018

Published: April 17, 2018

## REFERENCES

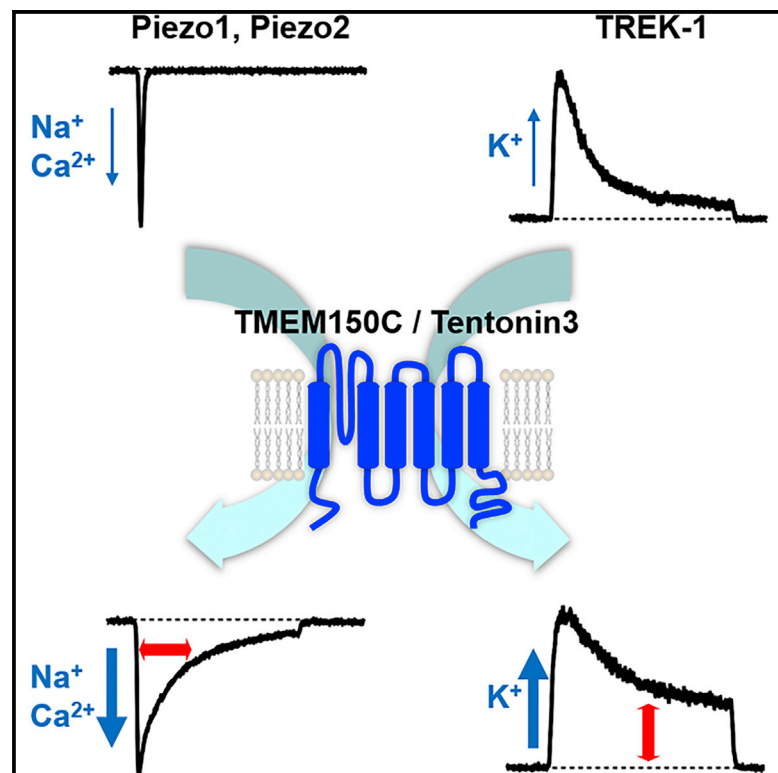
- Albuisson, J., Murthy, S.E., Bandell, M., Coste, B., Louis-Dit-Picard, H., Mathur, J., Fénéant-Thibault, M., Tertian, G., de Jaureguiberry, J.P., Syfuss, P.Y., et al. (2013). Dehydrated hereditary stomatocytosis linked to gain-of-function mutations in mechanically activated PIEZO1 ion channels. *Nat. Commun.* **4**, 1884.
- Alloui, A., Zimmermann, K., Mamet, J., Duprat, F., Noël, J., Chemin, J., Guy, N., Blondeau, N., Voilley, N., Rubat-Coudert, C., et al. (2006). TREK-1, a K<sup>+</sup> channel involved in polymodal pain perception. *EMBO J.* **25**, 2368–2376.
- Anderson, E.O., Schneider, E.R., and Bagriantsev, S.N. (2017). Piezo2 in cutaneous and proprioceptive mechanotransduction in vertebrates. *Curr. Top. Membr.* **79**, 197–217.
- Bae, C., Gnanasambandam, R., Nicolai, C., Sachs, F., and Gottlieb, P.A. (2013). Xerocytosis is caused by mutations that alter the kinetics of the mechanosensitive channel PIEZO1. *Proc. Natl. Acad. Sci. USA* **110**, E1162–E1168.
- Bagriantsev, S.N., Peyronnet, R., Clark, K.A., Honoré, E., and Minor, D.L., Jr. (2011). Multiple modalities converge on a common gate to control K2P channel function. *EMBO J.* **30**, 3594–3606.
- Bagriantsev, S.N., Clark, K.A., and Minor, D.L., Jr. (2012). Metabolic and thermal stimuli control K(2P)2.1 (TREK-1) through modular sensory and gating domains. *EMBO J.* **31**, 3297–3308.
- Besch, S.R., Suchyna, T., and Sachs, F. (2002). High-speed pressure clamp. *Pflugers Arch.* **445**, 161–166.
- Borbiro, I., and Rohacs, T. (2017). Regulation of Piezo channels by cellular signaling pathways. *Curr. Top. Membr.* **79**, 245–261.
- Borbiro, I., Badheka, D., and Rohacs, T. (2015). Activation of TRPV1 channels inhibits mechanosensitive Piezo channel activity by depleting membrane phosphoinositides. *Sci. Signal.* **8**, ra15.
- Brohawn, S.G., del Mármol, J., and MacKinnon, R. (2012). Crystal structure of the human K2P TRAAK, a lipid- and mechano-sensitive K<sup>+</sup> ion channel. *Science* **335**, 436–441.
- Brohawn, S.G., Su, Z., and MacKinnon, R. (2014). Mechanosensitivity is mediated directly by the lipid membrane in TRAAK and TREK1 K<sup>+</sup> channels. *Proc. Natl. Acad. Sci. USA* **111**, 3614–3619.
- Chung, J., Nakatsu, F., Baskin, J.M., and De Camilli, P. (2015). Plasticity of PI4KIII $\alpha$  interactions at the plasma membrane. *EMBO Rep.* **16**, 312–320.
- Clausen, M.V., Jarerattanachat, V., Carpenter, E.P., Sansom, M.S.P., and Tucker, S.J. (2017). Asymmetric mechanosensitivity in a eukaryotic ion channel. *Proc. Natl. Acad. Sci. USA* **114**, E8343–E8351.
- Comoglio, Y., Levitz, J., Kienzler, M.A., Lesage, F., Isacoff, E.Y., and Sandoz, G. (2014). Phospholipase D2 specifically regulates TREK potassium channels via direct interaction and local production of phosphatidic acid. *Proc. Natl. Acad. Sci. USA* **111**, 13547–13552.
- Coste, B., Mathur, J., Schmidt, M., Earley, T.J., Ranade, S., Petrus, M.J., Dublin, A.E., and Patapoutian, A. (2010). Piezo1 and Piezo2 are essential components of distinct mechanically activated cation channels. *Science* **330**, 55–60.
- Coste, B., Hough, G., Murray, M.F., Stitzel, N., Bandell, M., Giovanni, M.A., Philippakis, A., Hoischen, A., Riemer, G., Steen, U., et al. (2013). Gain-of-function mutations in the mechanically activated ion channel PIEZO2 cause

- a subtype of Distal Arthrogyriposis. *Proc. Natl. Acad. Sci. USA* **110**, 4667–4672.
- Cox, C.D., Bae, C., Ziegler, L., Hartley, S., Nikolova-Krstevski, V., Rohde, P.R., Ng, C.A., Sachs, F., Gottlieb, P.A., and Martinac, B. (2016). Removal of the mechanoprotective influence of the cytoskeleton reveals PIEZO1 is gated by bilayer tension. *Nat. Commun.* **7**, 10366.
- Dong, Y.Y., Pike, A.C., Mackenzie, A., McClenaghan, C., Aryal, P., Dong, L., Quigley, A., Grieben, M., Goubin, S., Mukhopadhyay, S., et al. (2015). K2P channel gating mechanisms revealed by structures of TREK-2 and a complex with Prozac. *Science* **347**, 1256–1259.
- Dubin, A.E., Murthy, S., Lewis, A.H., Brosse, L., Cahalan, S.M., Grandl, J., Coste, B., and Patapoutian, A. (2017). Endogenous Piezo1 can confound mechanically activated channel identification and characterization. *Neuron* **94**, 266–270.
- Florez-Paz, D., Bali, K.K., Kuner, R., and Gomis, A. (2016). A critical role for Piezo2 channels in the mechanotransduction of mouse proprioceptive neurons. *Sci. Rep.* **6**, 25923.
- Glogowska, E., Schneider, E.R., Maksimova, Y., Schulz, V.P., Lezon-Geyda, K., Wu, J., Radhakrishnan, K., Keel, S.B., Mahoney, D., Freidmann, A.M., et al. (2017). Novel mechanisms of PIEZO1 dysfunction in hereditary xerocytosis. *Blood* **130**, 1845–1856.
- Gottlieb, P.A., Bae, C., and Sachs, F. (2012). Gating the mechanical channel Piezo1: a comparison between whole-cell and patch recording. *Channels (Austin)* **6**, 282–289.
- Guo, Y.R., and MacKinnon, R. (2017). Structure-based membrane dome mechanism for Piezo mechanosensitivity. *eLife* **6**, e33660.
- Hao, J., and Delmas, P. (2011). Recording of mechanosensitive currents using piezoelectrically driven mechanostimulator. *Nat. Protoc.* **6**, 979–990.
- Hao, J., Padilla, F., Dandonneau, M., Lavebratt, C., Lesage, F., Noël, J., and Delmas, P. (2013). Kv1.1 channels act as mechanical brake in the senses of touch and pain. *Neuron* **77**, 899–914.
- Hong, G.S., Lee, B., Wee, J., Chun, H., Kim, H., Jung, J., Cha, J.Y., Riew, T.R., Kim, G.H., Kim, I.B., and Oh, U. (2016). Tentonin 3/TMEM150c Confers Distinct Mechanosensitive Currents in Dorsal-Root Ganglion Neurons with Proprioceptive Function. *Neuron* **91**, 708–710.
- Hong, G.S., Lee, B., and Oh, U. (2017). Evidence for mechanosensitive channel activity of Tentonin 3/TMEM150C. *Neuron* **94**, 271–273.
- Koser, D.E., Thompson, A.J., Foster, S.K., Dwivedy, A., Pillai, E.K., Sheridan, G.K., Svoboda, H., Viana, M., Costa, L.D., Guck, J., et al. (2016). Mechanosensing is critical for axon growth in the developing brain. *Nat. Neurosci.* **19**, 1592–1598.
- Lewis, A.H., and Grandl, J. (2015). Mechanical sensitivity of Piezo1 ion channels can be tuned by cellular membrane tension. *eLife* **4**, e12088.
- Lolicato, M., Riegelhaupt, P.M., Arrigoni, C., Clark, K.A., and Minor, D.L., Jr. (2014). Transmembrane helix straightening and buckling underlies activation of mechanosensitive and thermosensitive K(2P) channels. *Neuron* **84**, 1198–1212.
- Lolicato, M., Arrigoni, C., Mori, T., Sekioka, Y., Bryant, C., Clark, K.A., and Minor, D.L., Jr. (2017). K<sub>2P</sub>2.1 (TREK-1)-activator complexes reveal a cryptic selectivity filter binding site. *Nature* **547**, 364–368.
- Lukacs, V., Mathur, J., Mao, R., Bayrak-Toydemir, P., Procter, M., Cahalan, S.M., Kim, H.J., Bandell, M., Longo, N., Day, R.W., et al. (2015). Impaired PIEZO1 function in patients with a novel autosomal recessive congenital lymphatic dysplasia. *Nat. Commun.* **6**, 8329.
- Murthy, S.E., Dubin, A.E., and Patapoutian, A. (2017). Piezos thrive under pressure: mechanically activated ion channels in health and disease. *Nat. Rev. Mol. Cell Biol.* **18**, 771–783.
- Noël, J., Zimmermann, K., Busserolles, J., Deval, E., Alloui, A., Diocot, S., Guy, N., Borsotto, M., Reeh, P., Eschalièr, A., and Lazdunski, M. (2009). The mechano-activated K<sup>+</sup> channels TRAAK and TREK-1 control both warm and cold perception. *EMBO J.* **28**, 1308–1318.
- Pathak, M.M., Nourse, J.L., Tran, T., Hwe, J., Arulmoli, J., Le, D.T., Bernardis, E., Flanagan, L.A., and Tombola, F. (2014). Stretch-activated ion channel Piezo1 directs lineage choice in human neural stem cells. *Proc. Natl. Acad. Sci. USA* **111**, 16148–16153.
- Prato, V., Taberner, F.J., Hockley, J.R.F., Callejo, G., Arcourt, A., Tazir, B., Hammer, L., Schad, P., Heppenstall, P.A., Smith, E.S., and Lechner, S.G. (2017). Functional and molecular characterization of mechanoinensitive “silent” nociceptors. *Cell Rep.* **21**, 3102–3115.
- Qi, Y., Andolfi, L., Frattini, F., Mayer, F., Lazzarino, M., and Hu, J. (2015). Membrane stiffening by STOML3 facilitates mechanosensation in sensory neurons. *Nat. Commun.* **6**, 8512.
- Ranade, S.S., Woo, S.H., Dubin, A.E., Moshourab, R.A., Wetzel, C., Petrus, M., Mathur, J., Bégy, V., Coste, B., Mainquist, J., et al. (2014). Piezo2 is the major transducer of mechanical forces for touch sensation in mice. *Nature* **516**, 121–125.
- Ranade, S.S., Syeda, R., and Patapoutian, A. (2015). Mechanically activated ion channels. *Neuron* **87**, 1162–1179.
- Sandoz, G., Bell, S.C., and Isacoff, E.Y. (2011). Optical probing of a dynamic membrane interaction that regulates the TREK1 channel. *Proc. Natl. Acad. Sci. USA* **108**, 2605–2610.
- Saotome, K., Murthy, S.E., Kefauver, J.M., Whitwam, T., Patapoutian, A., and Ward, A.B. (2017). Structure of the mechanically activated ion channel Piezo1. *Nature* **554**, 481–486.
- Schewe, M., Nematian-Ardestani, E., Sun, H., Musinszki, M., Cordeiro, S., Bucci, G., de Groot, B.L., Tucker, S.J., Rapedius, M., and Baukrowitz, T. (2016). A Non-canonical voltage-sensing mechanism controls gating in K2P K(+) channels. *Cell* **164**, 937–949.
- Schneider, E.R., Mastrotto, M., Laursen, W.J., Schulz, V.P., Goodman, J.B., Funk, O.H., Gallagher, P.G., Gracheva, E.O., and Bagriantsev, S.N. (2014). Neuronal mechanism for acute mechanosensitivity in tactile-foraging waterfowl. *Proc. Natl. Acad. Sci. USA* **111**, 14941–14946.
- Schneider, E.R., Anderson, E.O., Mastrotto, M., Matson, J.D., Schulz, V.P., Gallagher, P.G., LaMotte, R.H., Gracheva, E.O., and Bagriantsev, S.N. (2017). Molecular basis of tactile specialization in the duck bill. *Proc. Natl. Acad. Sci. USA* **114**, 13036–13041.
- Suchyna, T.M., Markin, V.S., and Sachs, F. (2009). Biophysics and structure of the patch and the gigaseal. *Biophys. J.* **97**, 738–747.
- Syeda, R., Xu, J., Dubin, A.E., Coste, B., Mathur, J., Huynh, T., Matzen, J., Lao, J., Tully, D.C., Engels, I.H., et al. (2015). Chemical activation of the mechanotransduction channel Piezo1. *eLife* **4**, e07369.
- Syeda, R., Florendo, M.N., Cox, C.D., Kefauver, J.M., Santos, J.S., Martinac, B., and Patapoutian, A. (2016). Piezo1 channels are inherently mechanosensitive. *Cell Rep.* **17**, 1739–1746.
- Szczot, M., Pogorzala, L.A., Solinski, H.J., Young, L., Yee, P., Le Pichon, C.E., Chesler, A.T., and Hoon, M.A. (2017). Cell-type-specific splicing of Piezo2 regulates mechanotransduction. *Cell Rep.* **21**, 2760–2771.
- Woo, S.H., Lukacs, V., de Nooij, J.C., Zaytseva, D., Criddle, C.R., Francisco, A., Jessell, T.M., Wilkinson, K.A., and Patapoutian, A. (2015). Piezo2 is the principal mechanotransduction channel for proprioception. *Nat. Neurosci.* **18**, 1756–1762.
- Wu, J., Lewis, A.H., and Grandl, J. (2017a). Touch, tension, and transduction: the function and regulation of Piezo ion channels. *Trends Biochem. Sci.* **42**, 57–71.
- Wu, J., Young, M., Lewis, A.H., Martfeld, A.N., Kalmeta, B., and Grandl, J. (2017b). Inactivation of mechanically activated Piezo1 ion channels is determined by the C-terminal extracellular domain and the inner pore helix. *Cell Rep.* **21**, 2357–2366.
- Zhao, Q., Zhou, H., Chi, S., Wang, Y., Wang, J., Geng, J., Wu, K., Liu, W., Zhang, T., Dong, M.-Q., et al. (2018). Structure and mechanogating mechanism of the Piezo1 channel. *Nature* **554**, 487–492.

# Cell Reports

## TMEM150C/Tentonin3 Is a Regulator of Mechano-gated Ion Channels

### Graphical Abstract



### Authors

Evan O. Anderson, Eve R. Schneider, Jon D. Matson, Elena O. Gracheva, Sviatoslav N. Bagriantsev

### Correspondence

slav.bagriantsev@yale.edu

### In Brief

Mechano-gated ion channels are essential for somatosensation, proprioception, hearing, vasodilation, and axonal growth. Anderson et al. show that the transmembrane protein TMEM150C facilitates activity of mechano-gated ion channels from different classes: Piezo1/2 and the potassium-selective channel TREK-1. This study reveals a role for TMEM150C as an evolutionarily conserved regulator of mechano-sensitivity.

### Highlights

- TMEM150C is co-expressed with Piezo2 in somatosensory neurons
- TMEM150C prolongs the duration of mechano-current produced by Piezo1/2 and TREK-1
- TMEM150C is a general regulator of mechano-gated ion channels
- TMEM150C function is conserved among vertebrates



**Cell Reports, Volume 23**

**Supplemental Information**

**TMEM150C/Tentonin3 Is a Regulator  
of Mechano-gated Ion Channels**

**Evan O. Anderson, Eve R. Schneider, Jon D. Matson, Elena O. Gracheva, and Sviatoslav N. Bagriantsev**

## Supplemental data

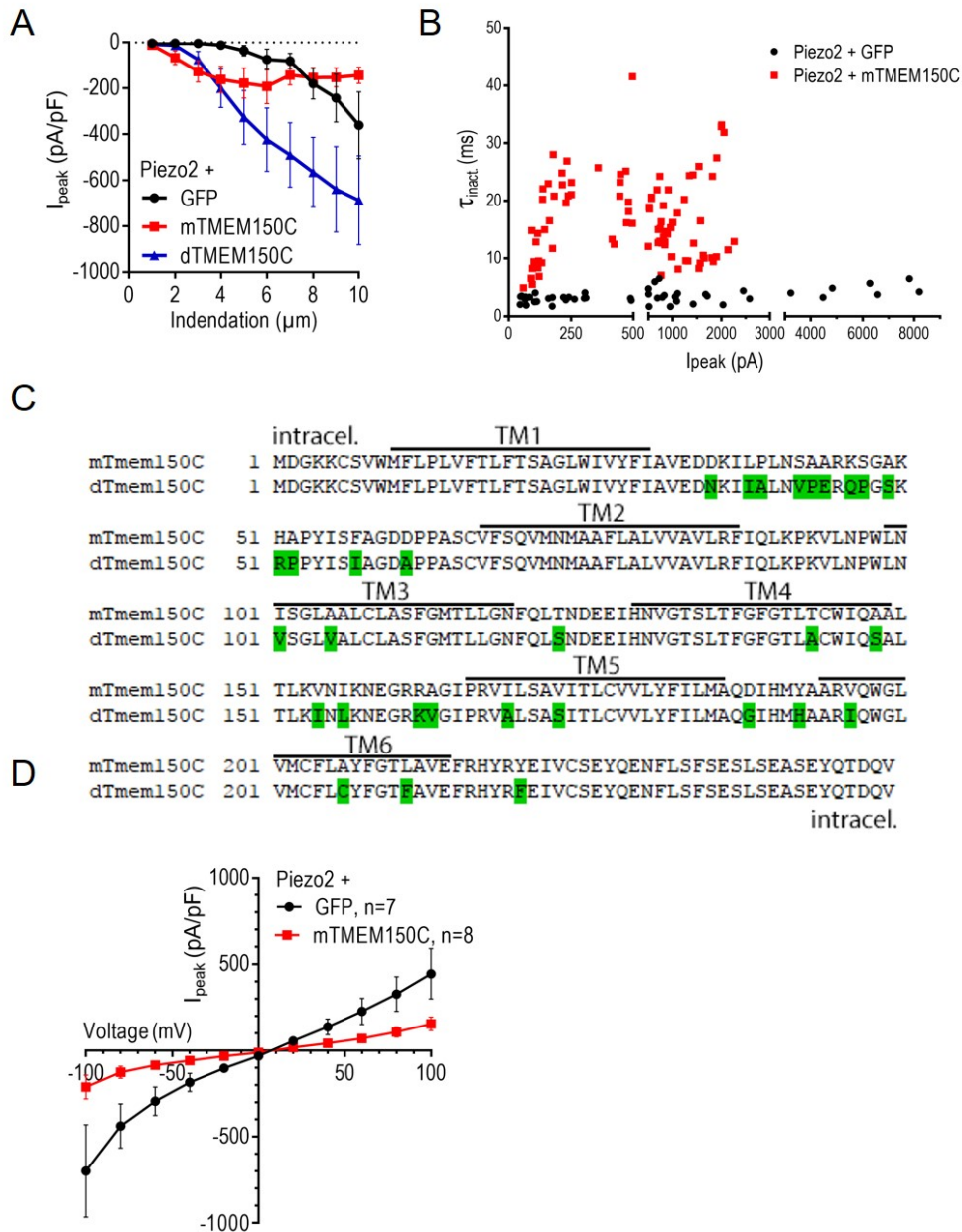


**Figure S1. Related to Figure 1.**

(A) Peak whole-cell MA current density measured in HEK293T<sup>ΔP1</sup> cells expressing Piezo2 with GFP or with mouse or duck TMEM150C ( $E_{\text{hold}} = -80$  mV) in response to mechanical indentations with a glass probe.

(B) TMEM150C prolongs Piezo2 MA current inactivation rate independently of peak current amplitude.

MA current inactivation rate measured at different peak MA current amplitudes in HEK293T<sup>ΔP1</sup> cells expressing Piezo2 with GFP or with mouse TMEM150C ( $E_{\text{hold}} = -80$  mV).

(C) Amino acid alignment of mouse TMEM150C (mTMEM150C, NP\_878261.1) and duck TMEM150C (dTMEM150C, MG697237). The proteins share 87% amino acid identity. Putative transmembrane domains are denoted by black bars.

(D) Peak MA current density-voltage plots measured in HEK293T<sup>ΔP1</sup> cells in response to mechanical indentation of 5-10  $\mu\text{m}$  for Piezo2+GFP and 4-9  $\mu\text{m}$  for Piezo2+mTMEM150C.

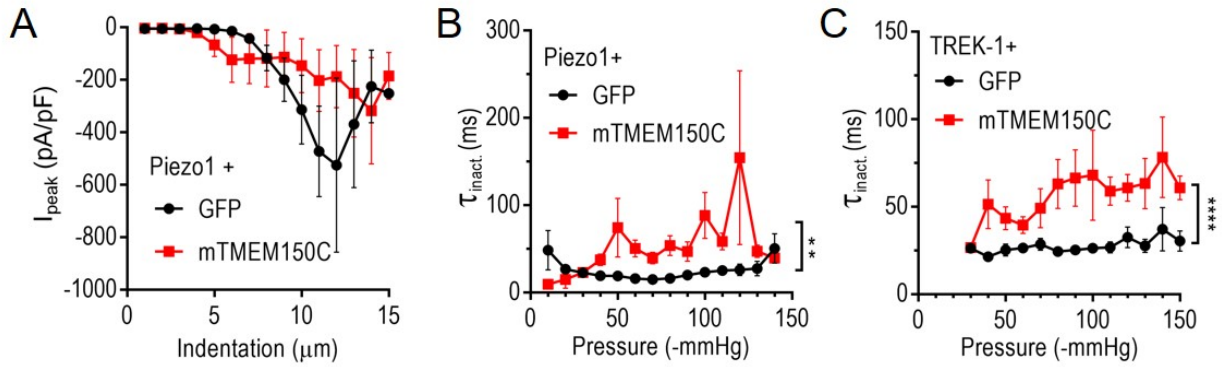


**Figure S2. Related to Figures 2, 3 and 4.**

(A) Peak whole-cell MA current density measured in HEK293T<sup>AP1</sup> cells expressing indicated constructs, in response to mechanical indentation with a glass probe at  $E_{\text{hold}} = -80$  mV.

(B and C) TMEM150C prolongs the rate of MA current inactivation in HEK293T<sup>AP1</sup> cells expressing Piezo1 (B) or TREK-1 (C). MA currents were elicited in the cell-attached mode by high-speed pressure clamp from a holding potential of -60 mV (Piezo1) or 0 mV (TREK-1).  $**P < 0.01$ ,  $****P < 0.0001$  for expression construct effect, two-way ANOVA.

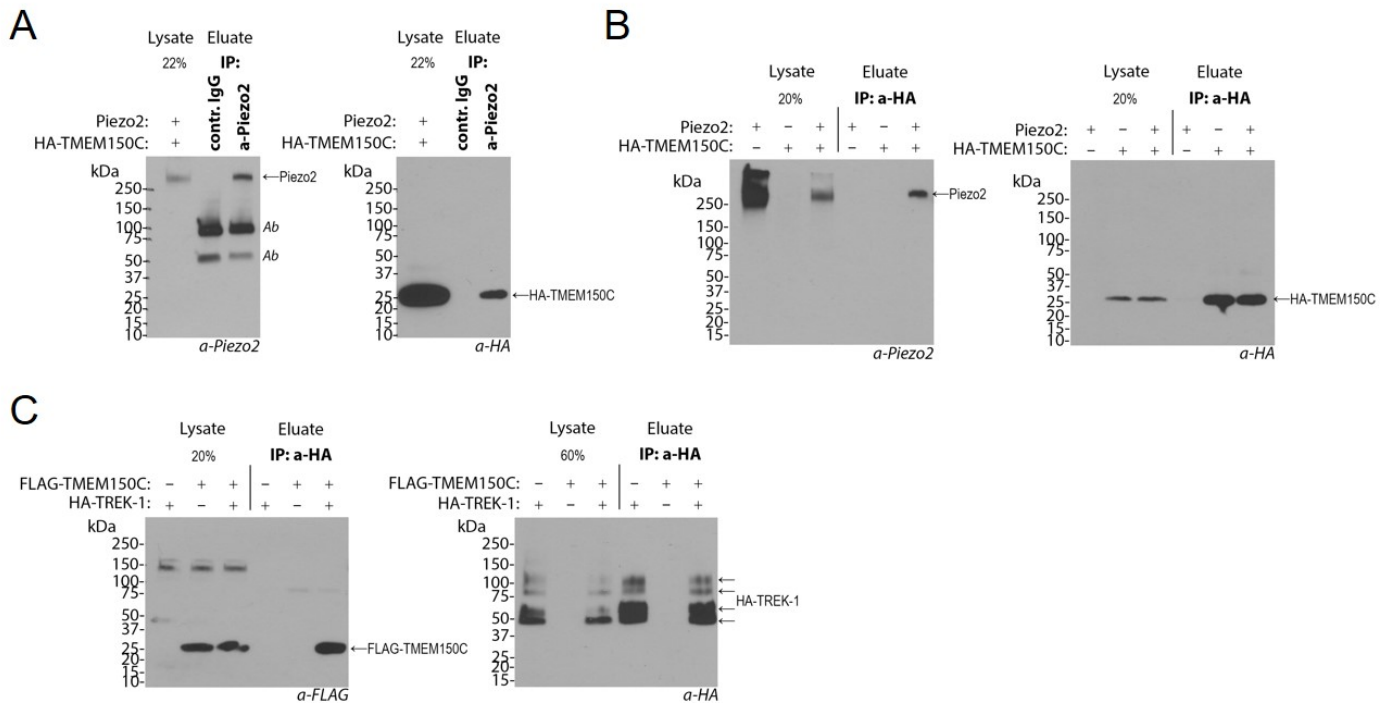


**Figure S3. Related to Figures 1 and 4.**

TMEM150C co-immunoprecipitates with Piezo2 and TREK-1 from HEK293T<sup>ΔPI</sup> lysates.

(A–C) Co-immunoprecipitation and immunoblot analysis of the indicated mouse proteins from detergent lysates of HEK293T<sup>ΔPI</sup> cells using antibodies immobilized on magnetic beads. Equal initial amounts of lysates were used for all immunoprecipitations. Percentages indicate the amount of lysate loaded on the gel relative to eluates. Calculated molecular weights for single subunits: Piezo2 (326 kDa), HA-TMEM150C (29 kDa), FLAG-TMEM150C (29 kDa), HA-TREK-1 (46 kDa). HA-TREK-1 migrates as four bands (bottom to top): monomer, glycosylated monomer, dimer, glycosylated dimer. *Ab*, antibody fragment from immunoaffinity beads.

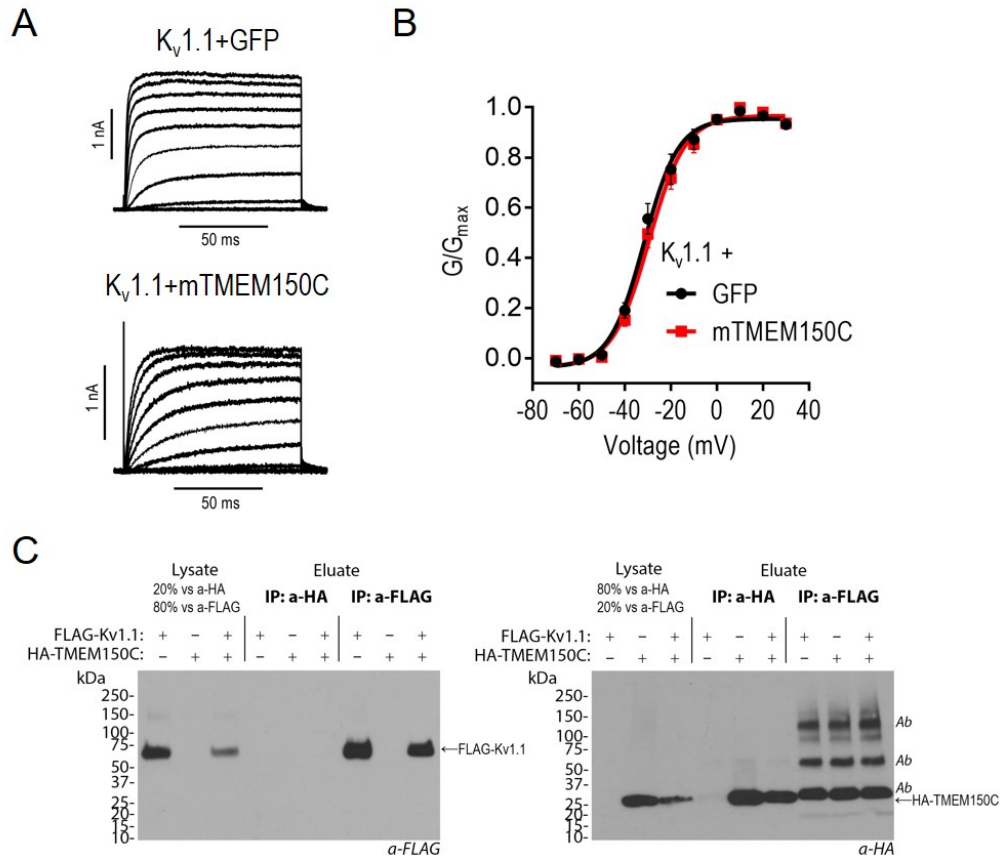


**Figure S4. Related to Figure 4.**

TMEM150C does not affect voltage dependence of activation of K<sub>v</sub>1.1.

(A) Exemplar whole-cell current families recorded from mouse K<sub>v</sub>1.1 in HEK293T<sup>ΔPI</sup> in the presence or absence of mouse TMEM150C in response to a voltage step protocol from -70 mV to 30 mV in 10 mV increments, from a holding potential of -70 mV.

(B) Normalized conductance from current families recorded from K<sub>v</sub>1.1 fit with a Boltzmann function.  $V_{1/2} = -31.7 \pm 0.9$  mV (K<sub>v</sub>1.1 + GFP, n = 13),  $-29.6 \pm 0.8$  mV (K<sub>v</sub>1.1 + mTMEM150C, n = 11).

(C) TMEM150C does not co-immunoprecipitate with K<sub>v</sub>1.1 from HEK293T<sup>ΔPI</sup> lysates. Equal initial amounts of lysates were used for all immunoprecipitations. Percentages indicate the amount of lysate loaded on the gel relative to eluates. Calculated molecular weights for single subunits: HA-TMEM150C (29 kDa), FLAG-K<sub>v</sub>1.1 (60 kDa). Ab, antibody fragment from immunoaffinity beads.

## Supplemental Experimental Procedures

### Resource table

REAGENT OR RESOURCE	SOURCE	IDENTIFIER
<b>Biological samples</b>		
Trigeminal ganglia from adult domestic duck (Mallard)	This paper	
<b>Deposited Data</b>		
Duck (Mallard) TMEM150C	This paper	MG697237
<b>Experimental Models: Organisms</b>		
Domestic duck (Mallard): <i>Anas platyrhynchos domesticus</i>	MarWin Farm (New Hartford, CT)	
<b>Experimental Models: cell lines</b>		
HEK293T <sup>PIEZO1</sup> <sup>-/-</sup> (HEK293T <sup>ΔP1</sup> )	Dr. Ardem Patapoutian (Scripps Research Institute) (Lukacs et al., 2015)	
<b>Oligonucleotides</b>		
Mouse TMEM150C cloning FWD GGCATGGACGGGAAGAAATGC	This paper	
Mouse TMEM150C cloning Rev CCAAGGACAAACTGTTGCTACACC	This paper	
Duck TMEM150C cloning and <i>in situ</i> probe FWD GGTATGGACGGGAAGAAATGC	This paper	
Duck TMEM150C cloning and <i>in situ</i> probe Rev GGCTACACCTGATCTGTCTGG	This paper	
<b>Recombinant DNA</b>		
Mouse-Piezo2-Sport6	Dr. Ardem Patapoutian (Scripps Research Institute) (Coste et al., 2010)	ADN28065.1
Mouse-Piezo1-pMO	This paper	ADN28064.1
Mouse-TMEM150C-IRES2-GFP	This paper	NP_878261.1
Mouse-HA-TMEM150C-IRES2-GFP	This paper	
Mouse-FLAG-TMEM150C-IRES2-GFP	This paper	
Duck-TMEM150C-IRES2-GFP	This paper	MG697237
Mouse-TREK-1-pMO	This paper	NP_034737.2
Mouse-HA-TREK-1-pMO	This paper	
Mouse- K <sub>v</sub> 1.1- Myc-FLAG-pCMV6	OriGene	MR222106
IRES2-GFP	Clontech	
<b>Antibodies</b>		

Anti-HA tag (mouse)	Sigma-Aldrich	clone HA7 #H3663
Anti-FLAG tag (rabbit)	Sigma-Aldrich	F7425
Anti-Piezo2 (rabbit)	(Schneider et al., 2017)	57-1
Secondary anti-mouse-HRP	ThermoFisher	31430
Secondary anti-rabbit-HRP	ThermoFisher	31458
<b>Software and Algorithms</b>		
Prism 7.01	Graph pad	
pCLAMP 10	Molecular Devices	
MATLAB R2014b	MathWorks	
IGOR Pro 6.37	WaveMetrics	

### Contact for Reagent and Resource Sharing

Further information and requests for resources and reagents should be directed to Sviatoslav Bagriantsev (slav.bagriantsev@yale.edu).

### Supplemental experimental procedures

**RNA *in situ* hybridization.** Trigeminal ganglia from adult birds were processed and developed with alkaline phosphatase-conjugated anti-digoxigenin Fab fragments as described previously (Schneider et al., 2014). Dissected TGs were fixed in 4% paraformaldehyde in phosphate-buffered saline for 2 hrs at 4°C, sectioned at 12-15 µm thickness and probed with digoxigenin-labeled cRNA generated using T7/T3 *in vitro* transcription from transcript fragments amplified from duck TG cDNA (see Resource Table for primers). Signal was developed with alkaline phosphatase-conjugated anti-digoxigenin Fab fragments.

**Molecular cloning.** Standard cloning techniques were used, and all plasmids were verified by full-length sequencing. Mouse TREK-1 (K<sub>2p2.1</sub>) with and without the human influenza hemagglutinin (HA) tag on the N-terminus was cloned from the pGEMHE vector (Bagriantsev et al., 2012) into the pMO vector for expression in mammalian cells. Mouse TMEM150C was cloned from dorsal root ganglia into the IRES2-GFP vector. Mouse TMEM150C sequence used here is identical to that published elsewhere (GenBank accession number NP\_878261.1)(Hong et al., 2016). Tagged versions of TMEM150C were made by adding the HA (YPYDVPDYA) or FLAG (DYKDDDDK) sequence to the N-terminus. Duck TMEM150C was cloned from adult duck trigeminal ganglia into IRES2-GFP. The sequence of duck TMEM150C was deposited to GenBank under the accession number (MG697237):

```
MDGKKCSVWMFLPLVFTLFTSAGLWIVYFIAVEDNKIIALNVPERQPGSKRPPYISIAGDAPPASCVFSQVMNMAAF
LALVVAVLRFIQLKPKVLNPWLVNLSGLVALCLASFGMTLLGNFQLSNDEEIHNVGTSLTFGFGTLACWIQSALTLLKI
NLKNEGRKVGIPRVALSASITLVCVLYFILMAQGIHMHAAARIQWGLVMCFLCYFGTFFAVEFRHYRFEIVCSEYQENF
LSFSESLSEASEYQTDQV
```

**Cell Culture.** HEK293T<sup>AP1</sup> cells were cultured in DMEM with 10% FBS, 1% Penicillin/Streptomycin, and 2 mM glutamine. Cells prepared for Piezo1 cell-attached recordings were transfected using Lipofectamine3000 (ThermoFisher) following manufacturer's instructions. For all other experiments, cells were co-transfected using Lipofecatmine2000 (ThermoFisher) according to the manufacturer's instructions.

Co-transfections were 2 µg of total plasmid at a mass ratio of 1:1 except for the following: 1.5 µg Mouse-Piezo2-Sport6 + 0.5 µg IRES2-GFP (for whole-cell); 1.5 µg Mouse-Piezo2-Sport6 + 0.5 µg Mouse-TMEM150C-IRES2-GFP (for whole-cell); 1.5 µg Mouse-Piezo2-Sport6 + 0.5 µg IRES2-GFP (for cell-attached); 0.5 µg TREK-1 + 1 µg IRES2-GFP + 0.5 µg pMO (for cell-attached); 0.5 µg TREK-1 + 1 µg Mouse-TMEM150C-IRES2-GFP + 0.5µg pMO (for cell-attached).

**Immunoprecipitation.** Cellular lysates were obtained by nutating HEK293<sup>AP1</sup> cells for 20 min at 4°C in Lysis Buffer (100 mM NaCl, 20 mM KCl, 20% (v/v) glycerol, 5 mM EGTA, 1% CHAPS (w/v), 10 mM HEPES/NaOH pH 7.4) supplemented with antiproteases (Sigma-Aldrich #11697498001) and cleared by centrifugation at 14,000 x g for 10 min at 4°C. For anti-HA and anti-FLAG tag pull downs, lysates (200 µg of total protein in 500 µl) were incubated with anti-HA or anti-FLAG magnetic beads for 1 hr at room temperature, following the manufacturer's instructions (Pierce #88838 for HA beads, Pierce #A36797 for FLAG beads). For anti-Piezo2 pull downs, lysates were incubated overnight at 4°C with polyclonal rabbit antibody against Piezo2 (#57-1) (Schneider et al., 2017) or control rabbit IgG (Sigma-Aldrich #I5006) covalently linked to magnetic beads, following the manufacturer's instructions (Pierce #88805). Beads were washed three times with 800 µl of Lysis Buffer, eluted in 100 µl of pre-heated to 95°C non-reducing Laemmli buffer with 1% SDS, and analyzed by Western blotting on a PVDF membrane using monoclonal mouse antibodies against the HA tag (Sigma-Aldrich #H3663), rabbit polyclonal antibodies against the FLAG tag (Sigma-Aldrich #F7425), or polyclonal rabbit antibodies against Piezo2 (#57-1) (Schneider et al., 2017). Signals from horseradish peroxidase-conjugated secondary antibodies were developed using the SuperSignal chemiluminescent substrate (ThermoFisher #34050) and detected on an X-ray film.

**Electrophysiology.** Transfected HEK293T<sup>AP1</sup> were plated onto matrigel-coated coverslips (BD Bioscience, Billerica MA, diluted 1:100 in PBS) the day following transfection (18-24 hrs). Cells were visualized using an Olympus BX51-WI with an Orca flash2.8 camera (Hamamatsu). Data were acquired using a Multi-clamp 700-B patch-clamp amplifier, Digidata 1500 digitizer (Molecular Devices) and pCLAMP software. Currents were low-pass filtered at 10 kHz. Recordings were not corrected for liquid junction potential.

For whole-cell recordings of mechano-activated currents from Piezo2 and Piezo1, data were collected at a sampling rate of 20 kHz using a 500 MΩ feedback resistor, as previously described (Schneider et al., 2017). Patch pipettes were made from 1.5 mm outer diameter borosilicate glass (Warner Instruments #G150F-3) using a P-1000 puller, and were fire polished to 1-4 MΩ tip resistance. Series resistance and membrane capacitance were compensated at 85%. Internal solution contained (mM): 133 CsCl, 5 EGTA, 1 CaCl<sub>2</sub>, 1 MgCl<sub>2</sub>, 10 HEPES, 4 Mg-ATP, 0.4 Na<sub>2</sub>-GTP, pH to 7.3 with CsOH. External solution contained (mM): 140 NaCl, 5 KCl, 10 HEPES, 2.5 CaCl<sub>2</sub>, 1 MgCl<sub>2</sub>, 10 glucose (pH 7.4 with NaOH). Cells were mechanically stimulated with a fire-polished, blunt glass probe (tip diameter ~2-4 µm) which was controlled by a pre-loaded Piezo actuator stack (Physik Instrumente GmbH, DE) set at an angle of 32° from the horizontal plane. After break-in, the glass probe was positioned at the surface of the cell, just before cell displacement of the cell membrane would be observed. Cells were stimulated in 1 µm, 150 ms steps with a velocity of 1000 µm/s with 5 s between sweeps. All data were acquired within 5 minutes of break-in.

For whole-cell recording of voltage activation of K<sub>v</sub>1.1, internal solution contained (mM): 150 KCl, 3 MgCl<sub>2</sub>, 5 EGTA, 10 HEPES, pH to 7.2 with KOH. External solution was identical to that described above. Cells were held at -70 mV for 50 ms and briefly stepped to -80 mV for 20 ms to assess cell parameters. Then they were held for 50 ms at -70 mV before being subjected to 100 ms voltage stimulation steps, ranging from -70 mV to 30 mV in 10 mV increments. Following stimulation, cells were returned to -70 mV before the next sweep. Leak current was subtracted online using the P/4 method on pCLAMP. Series resistance and membrane capacitance were compensated at 85%. Analyzed and representative traces are an average of 3 protocols. Currents were averaged over 88-98 ms of each voltage step and converted to conductance using the equation  $G = I / (V_m - E_K)$ , where  $G$  is the conductance,  $I$  is the averaged current,  $V_m$  is the membrane potential and  $E_K$  is the reversal potential for potassium calculated for the solutions used at -86.16 mV. The conductance data were normalized by the maximum conductance data and fit with the Boltzmann equation,  $G = G_{min} + (G_{max} - G_{min}) / (1 + \exp^{-(V_{1/2} - V_m)/k})$ , where  $G_{min}$  and  $G_{max}$  are minimal and maximal conductance, respectively,  $V_m$  is the voltage,  $V_{1/2}$  is the voltage at which the channels reached 50% of their maximal conductance, and  $k$  is the slope of the curve.

For cell-attached recordings of mechanically activated current by high-speed pressure clamp (HSPC), data was collected at a sampling rate of 10 kHz using a 5 GΩ feedback resistor. Patch pipettes were made similarly to whole-cell pipettes, but with a tip resistance of 0.7-2 MΩ. Pipette solution contained (mM): 130 NaCl, 5 KCl, 10 HEPES, 10 TEA-Cl, 1 CaCl<sub>2</sub>, 1 MgCl<sub>2</sub>, pH to 7.3 with NaOH. Bath solution contained (mM): 140 KCl, 10 HEPES, 1 MgCl<sub>2</sub>, 10 glucose, pH to 7.3 using KOH. Pressure control for seal formation and pressure stimulation protocols were controlled using a HSPC-1 high speed pressure clamp system (ALA Scientific Instruments). Cells were approached with a 10-20 mmHg positive pressure, and pressure was released to form a gigaseal. Following formation of the gigaseal, holding potential was set to -60 mV for Piezo1 recordings or 0 mV for TREK-1 recordings. Cells were subjected to stepwise, 200 ms negative pressure steps (Δ10 mmHg) preceded by a 500 ms pre-pulse at 5 mmHg to remove inactivation (Lewis and Grandl, 2015), with 3 seconds between stimuli.

Inactivation kinetics of mechano-evoked currents were determined by fitting current decay to a single-exponential decay function, as previously described (Schneider et al., 2017). Briefly, MA currents were fit to the following single-exponential decay equation:  $I = \Delta I * \exp(-t/\tau_{inact})$ , where  $\Delta I$  is the difference between peak MA current and baseline,  $t$  is the time from the peak current (the start of the fit), and  $\tau_{inact}$  is the decay constant. Summary  $\tau_{inact}$  from figures represent averages from traces with the top 75% of MA current, as previously quantified (Coste et al., 2010), unless described otherwise.

Post-stimulus whole-cell mechano current was quantified for each trace as the average of 20 ms of data 5 ms following the removal of stimulus. For cell-attached recordings, post-stimulus current was quantified for each trace as the average of 20 ms of data 150 ms after the removal of pressure stimulus, allowing for pressure readings to return to zero. Reported  $I_{peak}$ -normalized post-stimulus current is an average of traces which yielded 75% or more maximal peak current.

The apparent threshold of mechano activated current was determined as the first indentation to elicit a peak current greater than background noise, typically at least 40 pA above averaged baseline. Similarly, the apparent threshold of mechano activated current through HSPC stimulation was also the first pressure stimulation to elicit a peak current resolvable above background noise, typically at least 10 pA.

**Statistical Analysis.** Data were analyzed using a combination of Igor Pro 6.3 (Wavemetrics, converted from pCLAMP using TaroTools), Matlab (Mathworks), and GraphPad Prism 7.01 (GraphPad Software, Inc). Sample size and statistical tests are reported in figure legends. Statistical tests were chosen based on normality of distributions and variance equality, or lack thereof, and the number of samples. Data were reported as mean  $\pm$  SEM, significance displayed as not significant (NS),  $P > 0.05$ ,  $*P < 0.05$ ,  $**P < 0.01$ ,  $***P < 0.001$ ,  $****P < 0.0001$ .